Contents lists available at ScienceDirect

Transactions of Nonferrous Metals Society of China

36(2026) 1479−1492

www.tnmsc.cn

Atypical intrinsic Elinvar behavior of β Ti−22Nb−6Zr alloy in high and wide temperature range

Sergey DUBINSKIY [a,*], Alexandra BARANOVA [a], Galina MARKOVA [b], Anastasia ZELENINA [c,d], Lada KOLOTOVA [e], Sergey STARIKOV [f], Andrey KOROTITSKIY [g], Andrey BAZLOV [h], Sergey PROKOSHKIN [a], Vladimir BRAILOVSKI [i]

[a] National University of Science and Technology "MISIS", Laboratory of Shape Memory Alloys, 4 Leninskiy prospect, Moscow, Russia;

[b] Tula State University, Department of Engineering and Materials Science, 92 Lenina prospect, Tula, Russia;

[c] Moscow Institute of Physics and Technology, 9 Institutskiy per., Dolgoprudny, Russia;

[d] Joint Institute for High Temperatures of RAS, 13 Bd. 2 Izhorskaya Street, Moscow, Russia;

[e] National Research University Higher School of Economics, Faculty of Physics, 20 Myasnitskaya Street, Moscow, Russia;

[f] Interdisciplinary Centre for Advanced Materials Simulation, Ruhr University Bochum, Germany;

[g] National University of Science and Technology "MISIS", Department of Physical Metallurgy of Non-Ferrous Metals, 4 Leninskiy prospect, Moscow, Russia;

[h] National University of Science and Technology "MISIS", Ultrafine-grained Metallic Materials Laboratory, 4 Leninskiy prospect, Moscow, Russia;

[i] École de Technologie Supérieure, 1100 Notre-Dame Street West, Montreal, Canada

Abstract: The Elinvar behavior of Ti−22Nb−6Zr shape memory alloy was studied to determine the mechanism of such behavior and find the way to control this effect. The temperature dependences of elastic properties were studied using torsional pendulum experiments. The stability of phase composition was evaluated by X-ray diffraction analysis. Compression mechanical testing and classical atomistic simulations were used to confirm the obtained results on the macroscopic and atomic levels. The heating/cooling rate of ≥9 °C/min allows realization of the two-way Elinvar behavior in the 150−550 °C range with a temperature coefficient of f_r^2 ~10^{-5} $°C^{-1}$; this behavior is stable, repeatable, and independent of the β-phase state, whether the alloy has a polygonized dislocation substructure or a recrystallized structure. The study concludes that the Elinvar behavior observed is an intrinsic property of BCC β-phase.

Keywords: Elinvar behavior; β titanium alloys; shape memory alloys; torsional pendulum experiment; atomistic simulation

1 Introduction

Numerous works were performed on the composition optimization [1−3], in-depth phase transformation characterization [4−6], mechanical properties and surface properties evaluation [7−9] of metastable β Ti−Nb-based shape memory alloys, mainly because of their low Young's modulus and improved biomechanical and biochemical compatibility with bone tissues [10−12]. Recently, a novel aspect of their functional behavior, such as an independence (or anomalously weak temperature dependence) of the elastic modulus, known as the Elinvar effect, was observed in a Ti−22Nb−6Zr alloy (at.%) on cooling in the 550−150 °C temperature range [13,14].

A previous experimental study [14] concluded that commonly known factors underlying the Elinvar behavior, such as magnetic domain inter-

Corresponding author: *Sergey DUBINSKIY, Tel: +7(499)230-2862, E-mail: sdubinskiy@gmail.com

https://doi.org/10.1016/S1003-6326(26)67042-2

Received 29 October 2024; accepted 18 June 2025

1003-6326/© 2026 The Nonferrous Metals Society of China. Published by Elsevier Ltd & Science Press

This is an open access article under the CC BY-NC-ND license (http://creativecommons.org/licenses/by-nc-nd/4.0/)

actions [15−17], phase [18,19] and pre-martensitic transformation phenomena [20−23], high dislocation density [24−26], and anisotropy of the temperature dependence of elastic modulus in low-symmetry crystal lattices [22,27,28], were not responsible for such a behavior in this alloy. Furthermore, as recently reported in Ref. [29], the Elinvar effect in a high-entropy Co−25Ni−50 (HfTiZr) alloy is caused by a particular thermal behavior of the highly distorted body-centered cubic (BCC) crystal lattice, which is different from that of the conventional three-component alloys with an undistorted BCC lattice, such as Ti−22Nb−6Zr. These observations logically lead to the hypothesis that the observation in the Ti−22Nb−6Zr alloy is Elinvar behavior, i.e. it is caused uniquely by atomic interactions inherent in this specific crystal lattice (similarly to the theoretically predicted phenomenon in pure β-Ti [30]). This hypothesis is supported by the results of atomistic simulations of "pseudo-BCC" uranium-based alloys in Refs. [31,32] and the experiments carried out in Ref. [33].

It was also shown that the Ti−22Nb−6Zr alloy manifested the Elinvar effect only on cooling (one-way effect), while on heating, the Elinvar effect was prevented by the formation of isothermal ω_{iso}-phase [14]. It can thus be hypothesized that the two-way Elinvar effect (i.e., on both heating and cooling) can be obtained if the formation of the ω_{iso}-phase in this alloy is suppressed by applying appropriate time−temperature heating conditions, taking into account the kinetics of ω_{iso}-phase precipitation [34].

The aim of this work is therefore to study the mechanisms underlying the Elinvar behavior of the Ti−22Nb−6Zr alloy in the 150−550 °C range; to obtain a full-valued two-way Elinvar behavior; to quantify this effect using torsional pendulum experiments, classical atomistic simulations, and mechanical testing, accompanied with X-ray diffraction (XRD) structure and phase analysis; to evaluate the possibility of controlling this effect for practical applications. As a first step, the cyclic stability of the one-way Elinvar behavior was studied using torsional pendulum experiments with low heating/cooling rate. Next, the cooling/heating rate sensitivity of the Elinvar effect was studied and a minimum critical heating/cooling rate that produces the two-way Elinvar behavior was found. Then, the study of cyclic stability of the two-way Elinvar behavior was carried out using the previously found heating/cooling conditions which allowed a conclusion that such behavior is stable, repeatable and independent of the β-phase structural state, regardless of whether it is a polygonized dislocation substructure or a defect-free recrystallized grain structure. Moreover, molecular dynamic simulations were carried out which confirmed that the Elinvar behavior in the Ti−22Nb−6Zr alloy was the latter's intrinsic property determined by the elastic atomic interactions. Finally, mechanical compression tests were carried out, which validated that this alloy effectively manifests the two-way Elinvar behavior in the 150−550 °C range and thus opens a way for its practical applications.

2 Experimental

2.1 Materials and processing

An 8 kg ingot of Ti−22Nb−6Zr (at.%) alloy in which the atypical Elinvar effect was first reported in Ref. [14] was vacuum-arc melted using a DVV−125 furnace with low impurity content (O<0.05 wt.%, C<0.01 wt.%, N<0.01 wt.%, and H<0.01 wt.%) and then hot-forged at the I. P. Bardin Central Research Institute of Ferrous Metallurgy (Russia). Next, the ingot was subjected to homogenization annealing (HA) for 30 min at 1100 °C, cut into 20 mm × 10 mm × 50 mm using electronic discharge machine (EDM) billets, hot rolled at 1100 °C (HR), and once again subjected to homogenization annealing for 30 min at 1100 °C. The billet was then EDM cut into 2 mm × 10 mm × 50 mm plates, cold rolled with a true strain of ε=0.3, post-deformation annealed (PDA) and water cooled. Two PDA conditions were used in accordance with Ref. [35]: 30 min heating at 600 °C to form the polygonized dislocation substructure, i.e. P state (Fig. 1(a)), with a subgrain size of 100−300 nm and 30 min heating at 750 °C to form the recrystallized structure, i.e. R state (Fig. 1(b)). The average grain size in R state is estimated in the 10−20 μm range, based on Ref. [36]. After both PDAs, the alloy is in a single β-phase state without traces of any other phases [34,35,37]. The homogenization and post-deformation annealing procedures were carried out in argon atmosphere.

2.2 Torsional pendulum experiments

The dynamic shear modulus (G) and the tensile Young's modulus (E) are proportional to the squared resonance frequency (f_r^2) of torsional vibrations.

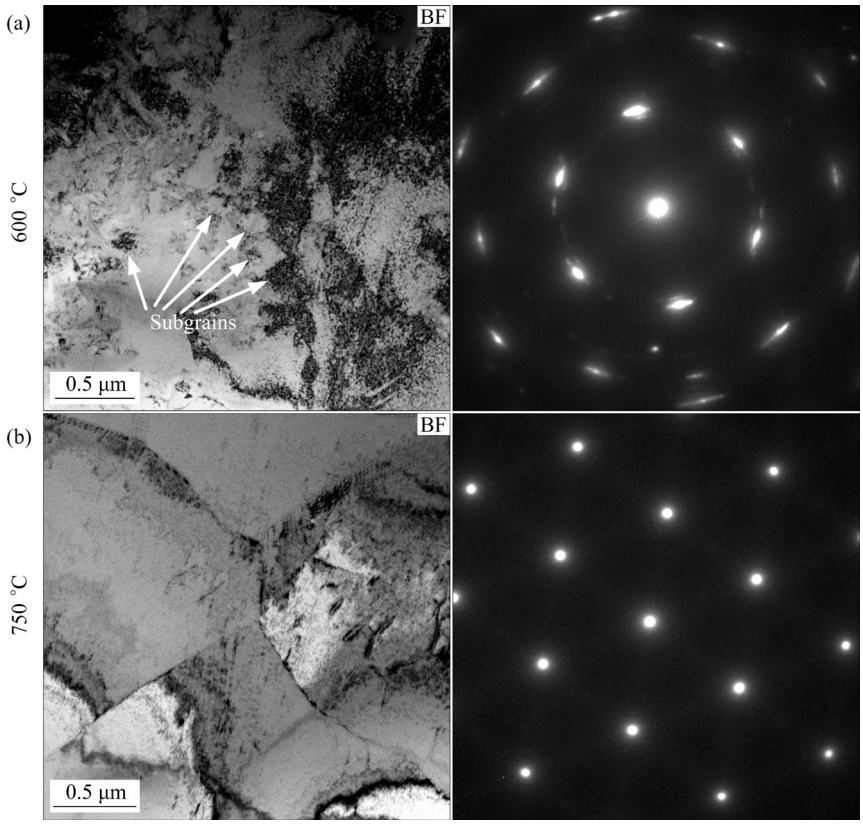

Fig. 1 Transmission electron microscopy (TEM) images and selected area electron diffraction (SAED) patterns ($\langle 111 \rangle_\beta$ zone axis) of Ti−22Nb−6Zr alloy in P (a) and R (b) states [35] (BF indicates bright field images; Low-angle azimuthal broadening of reflexes in (a) is caused by non-perfect lattice orientations in the highly dislocated selected area)

Therefore, the temperature dependence of the elastic properties (including the Elinvar behavior) can be studied by measuring the squared resonance frequency−temperature behavior calculated from an average value of the oscillation period (t) in the selected amplitude range [14]. In this work, the free-damped oscillation mode was used to measure the oscillation period on an RKM–TPI torsional pendulum in the room temperature (RT) to 550 °C temperature range with heating/cooling rates ranging from 2.5 to 20 °C/min. An average value of the oscillation period was calculated based on 5 values measured with a 5 °C step for the slowest heating/cooling rate (2.5 °C/min) and with a 25 °C step for all other rates. The specimens were 1.5 mm × 1.5 mm × 55 mm in size and had a working length of 45 mm. The strain amplitude for the torsional pendulum (γ) was about 3×10^{-5}, and the squared resonant frequency measurement error (f_r^2) was ±0.003 Hz^2. The temperature coefficients of f_r^2 (α_{fr}^2) during heating−cooling process in the studied temperature range were measured in the RT to 550 °C range using the least squares method. The value of the squared resonance frequency was calculated using the equation $f_r^2=1/\overline{t}^2$, where $\overline{t}$ is the average of 5 values of the oscillation period in s. Before measurements, the specimens were held in grips at 150 °C for 1 h to relieve stresses induced during installation. This relatively low holding temperature was selected to prevent any structure and phase transformations.

2.3 X-ray diffraction analysis

To determine the phase state after the heating and cooling cycles, X-ray diffraction analysis was carried out at RT using 8 mm × 10 mm × 1 mm and 8 mm × 10 mm × 2 mm specimens and a DRON−4 diffractometer with Cu K_α radiation. Before the analysis, the surface of the specimens was polished using P320−P1200 sandpaper and chemically etched in a HF + HNO_3 + H_2O solution with volume ratio of 1∶3∶6 to remove the oxidized and mechanically damaged layer. The lattice parameters of β-phase were calculated using the Nelson−Riley extrapolation.

2.4 Classical atomistic simulations

The molecular dynamics method (MD) was used to calculate the elastic properties [38−40].

Atomic interactions were described by the angle-dependent potential (ADP) developed for the Ti−Zr−Nb system. This potential is based on the previously published potential for Zr−Nb alloys [41]. The force matching method [42] was used to develop new potential functions as well as to make minor corrections to the Zr−Nb system potential. Details of the development and testing of the potential are largely similar to what was done in previous work [41,43].

Three elastic constants (c_{ij}) of the BCC lattice (c_{11}, c_{12} and c_{44}) were directly calculated using the Large-scale Atomic/Molecular Massively Parallel Simulator (LAMMPS) code [44]. Preparation of the simulated crystal was carried out under NPT conditions (i.e. an isothermal-isobaric ensemble) at normal pressure and a temperature varying from RT to the melting temperature. For the c_{11} and c_{12} elastic constants, $30a_0 \times 30a_0 \times 30a_0$ cubic cells were used, where a_0 is the equilibrium lattice parameter of the simulated alloy. For c_{44}, $70a_0 \times 70a_0 \times 70a_0$ cells were used (a_0 was changed from 3.292 to 3.337 Å). Such sizes of the simulation cells provide sufficient statistics in atomic vibrations during deformation. The elastic constants were calculated over the entire RT−melting temperature range. Both the Voigt (Young's modulus E_V; assuming homogeneous strain [45]) and Reuss (Young's modulus E_R; assuming homogeneous stress [46]) approximations were used to calculate the Young's modulus of β-alloy using the following Eqs. (1) and (2):

$$E_V = \frac{(c_{11} - c_{12} + 3c_{44})(c_{11} + 2c_{12})}{2c_{11} + 3c_{12} + c_{44}} \quad (1)$$

$$E_R = \frac{15c_{44}(c_{11} - c_{12})(c_{11} + 2c_{12})}{5c_{44}(c_{11} - c_{12}) + (c_{11} + 2c_{12})(4c_{44} + 3c_{11} - 3c_{12})} \quad (2)$$

The verification of the developed potential was realized by comparison with the data for pure β-titanium calculated in Ref. [30] (see Appendix A).

2.5 Mechanical testing

The static Young's modulus, the thermal expansion coefficient, and the Poisson's ratio (ν) were measured in the RT to 550 °C range using a deformation dilatometer (DIL 805 A/D) and specimens with cylindrical diameter of 5.5 mm and length of 10 mm. The heating/cooling rate between measurements was set as 10 °C/min. To ensure that the specimens remained in the elastic range without any traces of plastic strain, the applied stress was set below 100 MPa. The success of this approach was evidenced by a complete recovery of the specimens' dimensions at RT after two heating−cooling cycles and multiple loading−unloading cycles.

3 Results

3.1 Cyclic stability of Elinvar behavior at low heating/cooling rate (2.5 °C/min)

To verify whether thermal cycling with a low heating/cooling rate prevents a parasitic ω-phase peak in the heating half-cycle, the f_r^2−temperature dependence was monitored during 10 thermal cycles in the P state (Fig. 2). Starting from the first cycle, all heating curves showed pronounced peaks, with a maximum at ~375 °C, while cooling curves

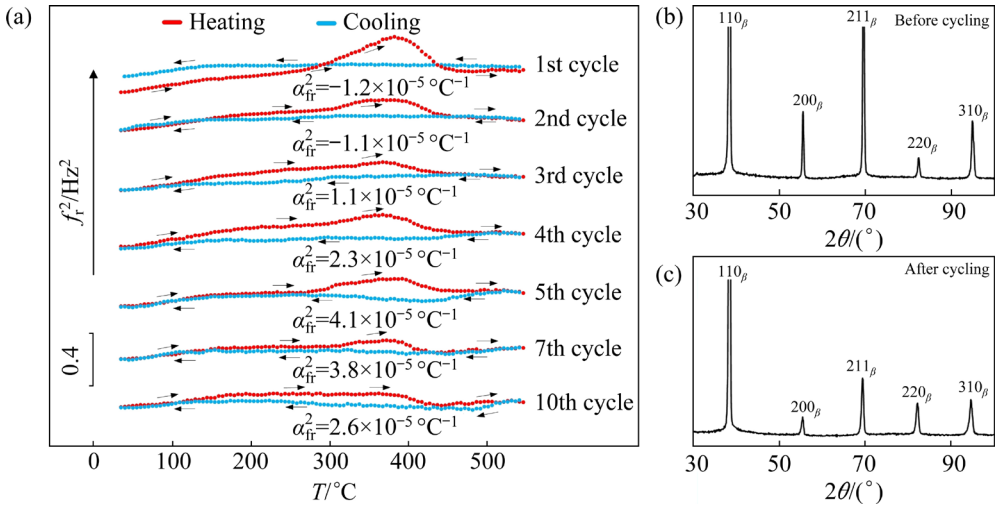

Fig. 2 Temperature dependence of f_r^2 in P state (ε=0.3, 600 °C, 30 min) of Ti−22Nb−6Zr alloy during thermal cycling (a) and XRD patterns before (b) and after (c) cycling

remained almost horizontal from 550 to 150 °C (the Elinvar behavior). A gradual reversible decrease of f_r^2 upon cooling and heating below 150 °C is attributable to the pre-martensitic softening phenomenon [14].

Pronounced peaks on the f_r^2 heating curves caused by the ω_{iso}-phase formation were already observed in the 300−450 °C range [14]. In the present work, thermal cycling leads to a gradual decrease of the peak area in this range during repetitive heating, but it is still visible after 10 thermocycles.

Because the Young's modulus and f_r^2 normally decrease with an increase in temperature, the normal sign of the temperature coefficient is negative and corresponds during cooling in the 550−150 °C (ΔT=400 °C) range to α_{fr}^2=−1.2×10^{-5} °C^{-1} for the 1st cycle and 2.6×10^{-5} °C^{-1} for the 10th cycle (Fig. 2), thus staying within the temperature coefficient limits of a commercially available Elinvar NI-SPAN-C alloy 902 [16].

To assess the phase composition changes during a 2.5 °C/min rate thermal cycling, an X-ray diffraction analysis of the Ti−22Nb−6Zr samples was performed at RT before and after each cycle (Fig. 2). Figure 2 shows the presence of only {110}, {200}, {211}, {220}, and {310} β-phase peaks, indicating that the phase composition at RT in the P structure state remains stable during cycling.

3.2 Heating/cooling rate sensitivity of Elinvar behavior

Since slow thermal cycling did not lead to a disappearance of the ω_{iso}-phase formation, experiments at higher heating/cooling rates were carried out in an attempt to suppress this phenomenon and obtain the two-way Elinvar effect.

The torsional pendulum experiment for both structure states of the Ti−22Nb−6Zr alloy was repeated at heating/cooling rates ranging from 2.5 to 20 °C/min, with intermediate steps of 6−7 and 8−9 °C/min (Fig. 3). When the thermal cycling rates were increased, the heating curves showed a decrease in the peak area corresponding to the ω_{iso}-phase formation (300−450 °C). The heating curves with a rate of 6−7 °C/min continued to have a slight f_r^2 peak in the 280−450 °C range, while starting from 8−9 °C/min, the heating curves became almost completely horizontal in the 150−550 °C range. Thus, an increase in the heating/cooling rate suppressed the ω_{iso}-phase formation and led to the realization of the two-way Elinvar effect in the 150−550 °C range. The temperature coefficients of f_r^2 upon cooling and heating at a rate of 20 °C/min were close and equal to −6.5×10^{-5} °C^{-1} for the P state and −5.3×10^{-5} °C^{-1} for the R state.

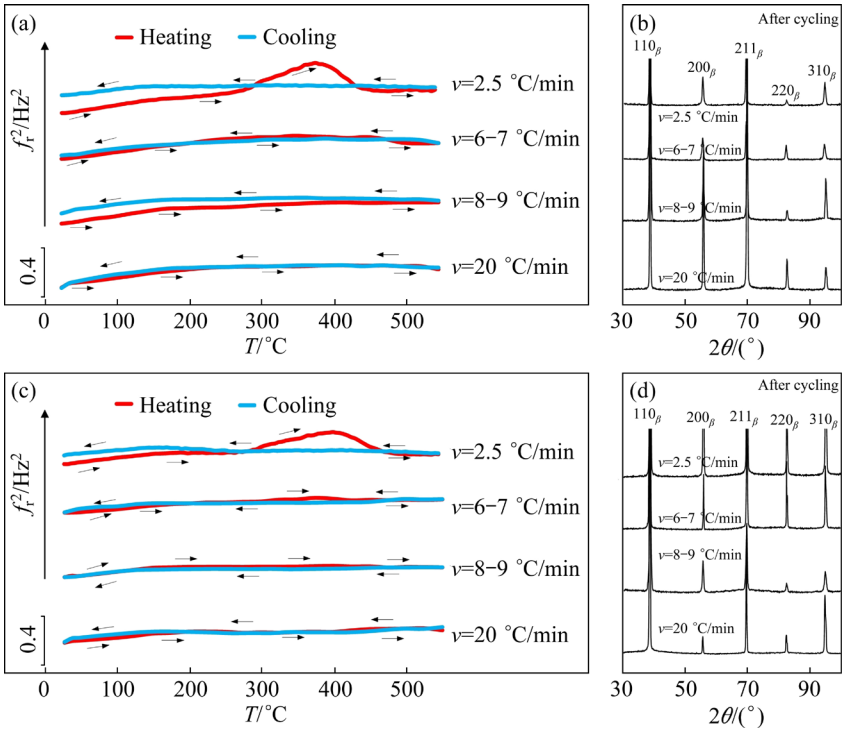

Fig. 3 Temperature dependence of f_r^2 in P (ε=0.3, 600 °C, 30 min) (a) and R (ε=0.3, 750 °C, 30 min) (c) states during thermal cycling with various heating/cooling rates, and XRD patterns after each cycle in P (b) and R (d) states

The XRD patterns obtained at RT before and after the experiment on the torsional pendulum at various heating/cooling rates shown in Fig. 3 indicate that for both structure states, P and R, the phase composition corresponded to BCC β-phase and remained unchanged, regardless of the heating/cooling rate.

3.3 Cyclic stability of Elinvar behavior at high heating/cooling rate of 20 °C/min

The torsional pendulum cycling experiment with a heating/cooling rate of 20 °C/min was repeated 10 times (Fig. 4) and showed a stable two-way Elinvar behavior. For the P and R structure states, temperature coefficients of f_r^2 during heating/cooling in the 150−550 °C (ΔT=400 °C) range were in the 10^{-5} °C^{-1} order of magnitude (see Table 1). Pre-martensitic lattice softening-related effects were observed during thermal cycling as a reversible decrease of the elastic modulus and f_r^2 during cooling towards Martensite start temperature M_s (approximately −20 °C [37]) and a reverse increase of the elastic modulus and f_r^2 during heating in the temperature range below 150 °C.

The X-ray diffraction analysis at RT after the 10th thermal cycle at a heating/cooling rate of 20 °C/min confirmed the presence of only BCC β-phase in both structures (Fig. 4). The diffraction peak profiles are symmetrical, and their widths are the same as in the initial conditions.

3.4 Validation of Elinvar behavior in Ti−22Nb−6Zr alloy with atomistic simulation and mechanical testing

To complement previous observations of the Elinvar behavior using a torsional pendulum, numerical simulations at the atomic level and mechanical tests at the macroscopic level were carried out. The first approach clarifies the physical principles of the effect, whereas the second approach opens up the possibilities for practical applications.

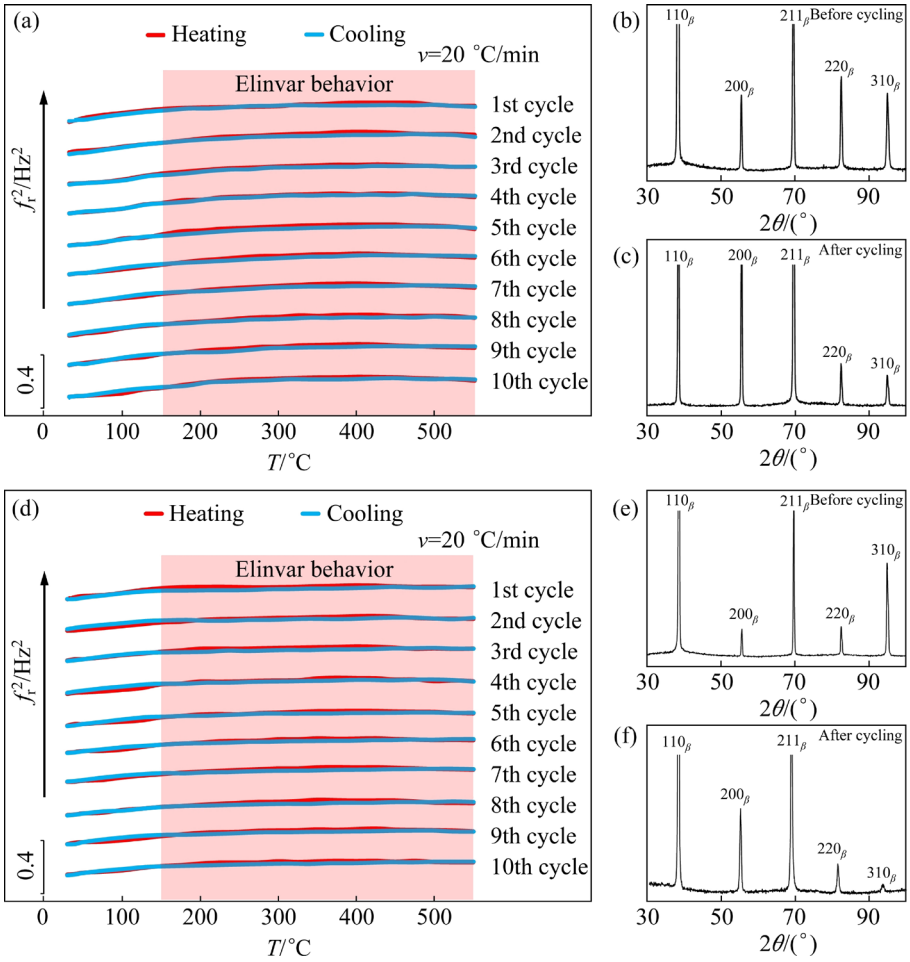

Fig. 4 Temperature dependence of f_r^2 in P (ε=0.3, 600 °C, 30 min) (a) and R (ε=0.3, 750 °C, 30 min) (d) states during thermal cycling at high heating/cooling rate (20 °C/min), and XRD patterns before and after cycling in P (b, c) and R (e, f) states

Table 1 Temperature coefficients of f_r^2 (α_{fr}^2) during thermal cycling in 550−150 °C range (10^{-5} °C^{-1})

Cycle	P state		R state	
	Heating	Cooling	Heating	Cooling
1st	4.9	7.0	1.2	5.1
2nd	6.1	6.8	5.4	1.7
3rd	5.5	6.1	4.7	6.7
4th	5.1	7.4	4.8	3.8
5th	3.3	6.0	6.2	4.9
6th	8.0	7.7	7.2	6.8
7th	7.3	8.1	7.2	5.1
8th	7.7	7.5	5.9	5.7
9th	8.0	7.4	7.6	5.2
10th	7.2	7.0	6.0	6.4

3.4.1 Classical atomistic simulations

The temperature dependencies of the elastic constants c_{11}, c_{12}, and c_{44} of the Ti−22Nb−6Zr β-alloy were calculated using the MD simulations (see Fig. 5(a)). It can be observed that in the 150−550 °C (ΔT=400 °C) range, when the temperature increases, c_{11} slightly increases, c_{12} slightly decreases, while c_{44} remains almost unchanged. This temperature range corresponds to that the Elinvar behavior was experimentally observed.

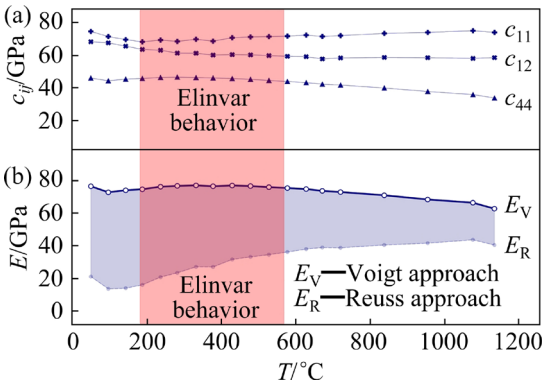

Fig. 5 Temperature dependences of c_{11}, c_{12} and c_{44} constants (a), and Young's modulus (b) of β-phase in Ti−22Nb−6Zr alloy calculated using Voigt and Reuss approximations

Based on the obtained c_{11}, c_{12}, and c_{44} values, the temperature dependencies of the Young's modulus of the Ti−22Nb−6Zr alloy were calculated using the Voigt and Reuss approaches and are plotted in Fig. 5(b). In the Voigt approach, changes in the Young's modulus on heating are much smaller than those occurring in the Reuss approach. In addition, the Voigt approach predicts a more traditional behavior of the Young's modulus outside the temperature range of the Elinvar effect: its value decreases with the increase of temperature. These results indicate that for Ti-based alloy systems, an approximation of the stress homogeneity (Reuss) is less suitable than that of the strain homogeneity (Voigt), which was also demonstrated in Refs. [47−49]. The temperature coefficient of the Young's modulus in the 150−550 °C range calculated with the Voigt approach corresponds to α_{fr}^2=−6.7×10^{-5} °C^{-1}, which supports the experimental observations. It is important to note that in the simulation, β-phase was considered as a stable structure over the entire temperature range of calculations, which makes it impossible to simulate the experimentally observed pre-martensitic lattice softening below 150 °C.

3.4.2 Mechanical testing results

To experimentally confirm the Elinvar behavior observed in the P and R states of the Ti−22Nb−6Zr alloy, the temperature dependence of the static Young's modulus was studied using a deformation dilatometer in compression mode. The sample strains were recorded along two axes: (1) in the compression direction and (2) in the direction perpendicular to the compression axis. The sample widening in the direction perpendicular to the compression axis was used to calculate the Young's modulus. Figure 6 illustrates that the Young's modulus remains constant (within the accuracy range of the measurement method) in the 150−550 °C range during the first (Figs. 6(a, c)) and second (Figs. 6(b, d)) heating−cooling cycles. It is noted that the obtained value of E=(110±10) GPa is a static "engineering" apparent elastic modulus which depends on the crystallographic texture and loading scheme, and thus cannot be directly compared to its dynamical "physical" equivalent determined using a torsional pendulum experiment or numerical simulation.

For a complete assessment of the elastic behavior of the Ti−22Nb−6Zr alloy in the P and R states, temperature dependences of the Poisson's ratio (ν) were also measured using the same equipment and provided constant values of ν=0.41±0.03 (P state) and ν=0.32±0.04 (R state). While in the R state, the Poisson's ratio was close to that of pure titanium (ν=0.30−0.33), and was 23% lower than that in the P state, which therefore calls for additional investigations.

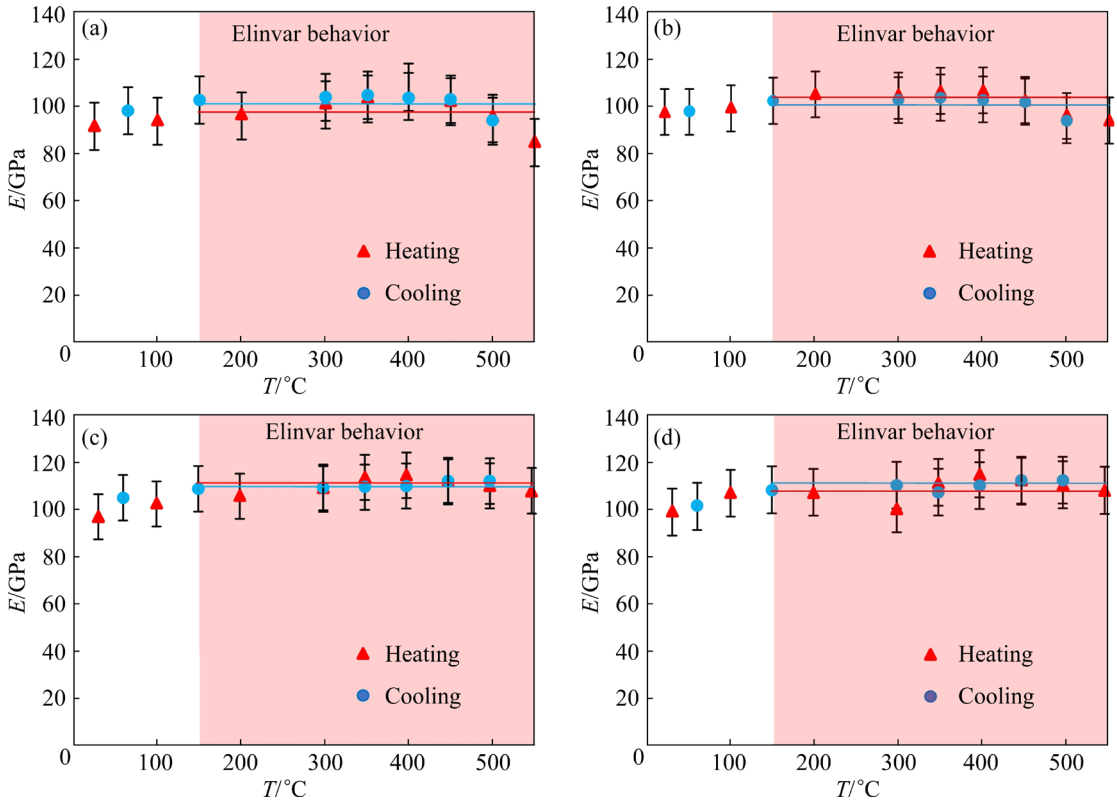

Fig. 6 Temperature dependence of Young's modulus (E) of Ti−22Nb−6Zr alloy in P (ε=0.3, 600 °C, 30 min) (a, b) and R (ε=0.3, 750 °C, 30 min) (c, d) states during mechanical testing: (a, c) 1st thermal cycle; (b, d) 2nd thermal cycle

Since the Elinvar effect is often accompanied by the Invar effect [28,50], which consists of a close-to-zero coefficient of the linear thermal expansion coefficient (α), specimens' elongations during thermal cycling were also measured in this study and showed a linear thermal expansion coefficient of 9×10^{-6} °C^{-1}, which is typical for titanium alloys.

4 Discussion

First and foremost, it should be noted that in all the experiments, the only phase observed before and after each heating−cooling cycle was β-phase, as demonstrated by the X-ray diffraction analysis. To assess the composition stability of β-phase during all the experiments, the BCC β-phase lattice parameter (a_β) and the half-height width (B_{hkl}) of the $\{110\}_\beta$ and $\{211\}_\beta$ X-ray diffraction lines were measured, and are shown in Fig. 7. It can be seen that the lattice parameter a_β remains constant after thermal cycling, regardless of the initial structural state of the β-phase, the heating/cooling rate or the number of cycles. The half-height widths B_{110_β} and B_{211_β} do not exceed the initial values during all testing sequences for each structural state of the Ti−22Nb−6Zr alloy. The half-height width (B_{hkl}) for the P state is generally somewhat higher than that for the R state as a result of the nano-scaled substructure, with a higher density of sub-boundaries and dislocations in the P state as compared to the defect-free R state. Furthermore, it can be assumed from Fig. 7 that the B_{hkl} after thermal cycles with slow rate (2.5 °C/min) increases especially from 7th to 10th cycle. It can be a result of lattice defects accumulation during multiple $\beta\rightarrow\omega\rightarrow\beta$ phase transformations. However, such increase does not exceed the tolerances of initial state before any heating−cooling experiment (see the pink area for P state and blue area for R state). The stability of the β-phase lattice parameter (a_β) and the half-height width (B_{hkl}) confirms the stability of β-phase during all the experiments, regardless of the number of cycles or the heating/cooling rates applied.

Thermal cycling of the Ti−22Nb−6Zr alloy (P state) in the RT↔550 °C range with a low heating/cooling rate (2.5 °C/min) does not lead to the Elinvar behavior upon heating because the ω_{iso}-phase particles have time to form and dissolve during each thermal cycle [14]. It is notable that after each

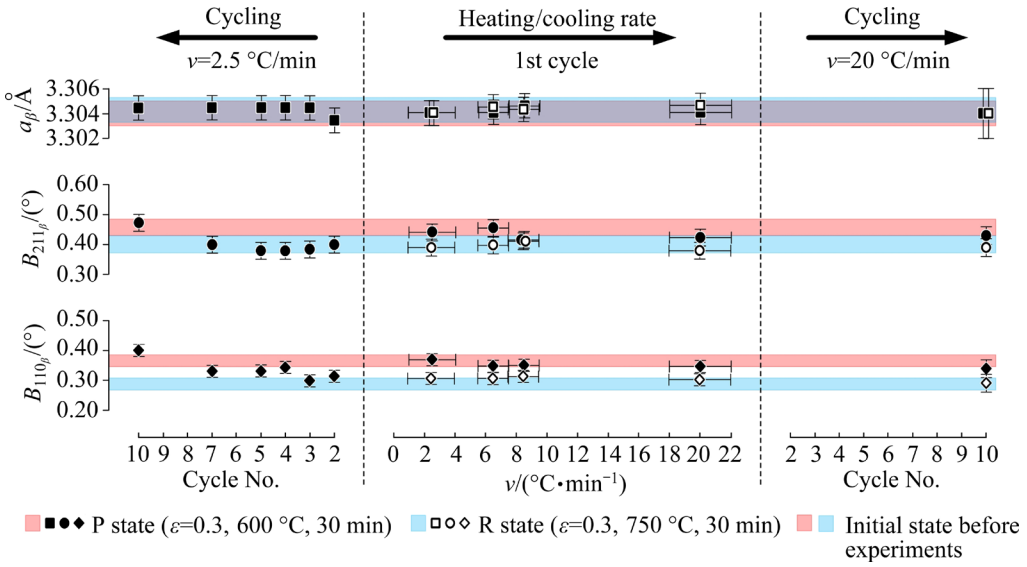

Fig. 7 Lattice parameter (a_β) and half-height widths (B_{hkl}) of β-phase in P and R states of Ti−22Nb−6Zr alloy at RT before and after heating−cooling cycles

subsequent heating−cooling cycle, the peak corresponding to the ω_{iso}-phase formation decreases, and this decrease is the most intensive from the 1st to the 3rd cycles (Fig. 2).

In an attempt to suppress the ω_{iso}-phase formation, obtain a stable β-phase, and thus provide a full-value two-way Elinvar effect, the heating/cooling rate was increased. As shown in Fig. 3, increasing the heating rate to 8−9 °C/min (critical value) and higher suppressed the ω_{iso}-phase formation by gradually limiting the time available for the ω_{iso}-phase precipitation. At and above this critical heating/cooling rate, the two-way Elinvar behavior was therefore obtained in the 150−550 °C range, which is confirmed by the numerical simulations. Furthermore, it is shown that the obtained two-way Elinvar behavior is stable in both structure states and repeatable for up to at least 10 thermal cycles at critical and higher heating/cooling rates, with no effect on the stability of β-phase.

Since the atomistic simulations and the mechanical testing directly provide information on the temperature dependence of Young's modulus, the results of the torsional pendulum experiments were also converted to the Young's modulus values using the method described in Appendix B. In Fig. 8, the temperature dependencies of the Young's modulus (E) from the atomistic simulations (Voigt approximation), from the pendulum experiments (at a critical heating/cooling rate of 9 °C/min) and from the compression testing (at a heating/cooling rate of 10 °C/min) are plotted altogether. It is noted that since the atomistic simulations did not consider the presence of lattice defects and were carried out for single β-phase state, their results can be compared only to the experiment in which the Ti− 22Nb−6Zr alloy in the R state was used at cooling/ heating rates, suppressing any phase transformation, i.e. when the alloy was in a pure coarse-grained β-phase state.

In the physical experiments and atomistic simulations, the Young's modulus of β-phase in the temperature range of the Elinvar behavior remains almost constant and corresponds to (75±3) GPa. The

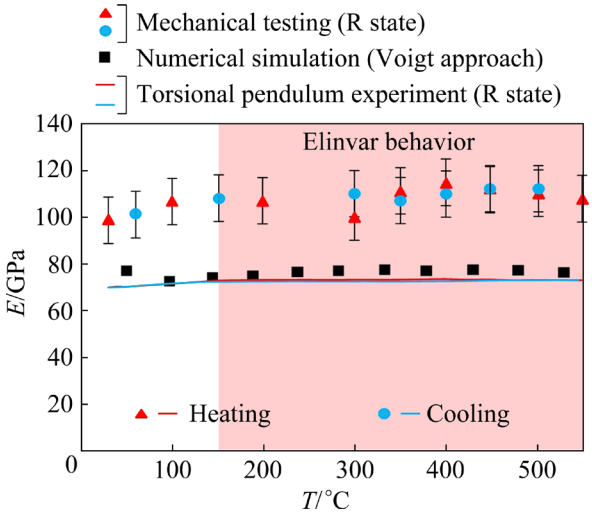

Fig. 8 Temperature dependencies of Young's modulus (E) of Ti−22Nb−6Zr alloy in R state obtained from mechanical testing, torsional pendulum experiments and atomistic simulations using Voigt approach

"engineering" apparent elastic modulus of β-phase during mechanical testing is higher than that from the torsional pendulum experiment for the reasons discussed in Section 3.4.2, but is also almost temperature independent. Therefore, it can be concluded that the Elinvar behavior observed in this study is an inherent property of β-phase similar to that in pure titanium [30]. Consequently, this behavior must be regarded as an "intrinsic" Elinvar behavior inherent to the β crystal lattice of this alloy. It is also noteworthy that such an Elinvar behavior could be observed not only in physical experiments (torsional pendulum) and atomistic simulations, but also during mechanical testing of macroscopic specimens. Furthermore, the cyclic stability of this effect opens up possibilities for its practical applications, providing that the heating/cooling rate is not lower than 9 °C/min.

Since the Ti−22Nb−6Zr alloy is not the only metallic material manifesting the Elinvar behavior, it is worthwhile to compare the temperature dependence of the normalized Young's modulus (E/E_0) (E_0 is the Young's modulus at RT) of this alloy with E/E_0 dependences of other metallic materials with low temperature sensitivity of their elastic behavior. To this end, Fig. 9 compares temperature dependences of the materials exhibiting the same phenomenon of low temperature sensitivity of their elastic characteristics, but caused by different physical or structural mechanisms: magnetic, phase transformation, high dislocation density and low crystallographic lattice symmetry.

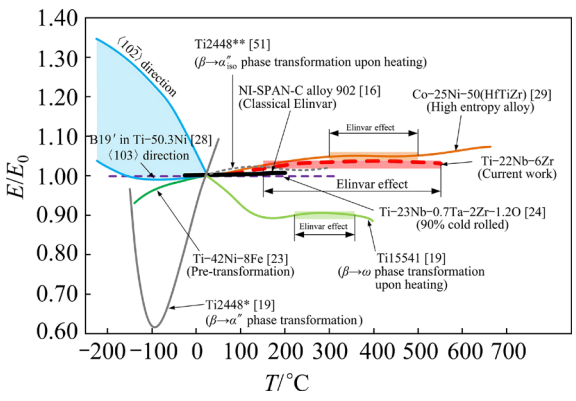

Fig. 9 Relative Young's modulus (E/E_0) vs temperature of metastable β Ti−22Nb−6Zr alloy compared with other metallic materials from Refs. [16,19,23,24,28,29,51] (The results for Ti2448 alloy from different sources are significantly different: Ref. [19] marked by * and Ref. [51] marked by **)

Firstly, Fig. 9 shows three alloys with relatively low temperature variations of their elastic characteristics caused by (1) pre-transformation and phase transformation phenomena or (2) low-symmetry lattices [28]. The first group is represented here by the Ti−42Ni−8Fe [23], Ti2448 [19,51] and Ti15541 [19] alloys. However, as can be seen, temperature variations of the elastic moduli of these alloys are generally significant, which remove them from consideration as Elinvar materials. The one exception is the Ti2448 alloy, where the elastic behavior significantly depends on the transformation type. The elastic behavior reported in Ref. [19] during reversible $\beta\leftrightarrow\alpha''$ phase transformation upon both heating and cooling is still far from the Elinvar type (it marked by "*" in Fig. 9). While in Ref. [51], it was shown that some Elinvar type behavior can be obtained only upon heating at about 300 °C due to $\beta\rightarrow\alpha''_{iso}$ transformation (marked by "**" in Fig. 9). The second group is represented here by Ti−50.3Ni alloy with low-symmetry monoclinic B19′-martensite (composition estimated using martensite finish temperature M_f−concentration dependence from Ref. [52]). In this alloy, the Elinvar behavior can be obtained in the $\langle 103\rangle_{B19'}$ direction in the temperature range from −200 to 0 °C, while in other directions, the elastic properties exhibit normal temperature dependence, meaning that the practical use of this alloy as an Elinvar material is limited.

Furthermore, both classical Ni−SPAN-C902 [16] (magnetic nature of the Elinvar behavior) and high-entropy Co−25Ni−50(HfTiZr) [29] (highly distorted BCC crystal lattice) alloys manifest excellent temperature stabilities, the former in the temperature range from −20 to 200 °C and the latter, in the temperature range from 300 to 500 °C. However, the temperature ranges within which the elastic properties of both alloys remain stable (~200 °C) are almost 50% narrower than that of the Ti−22Nb−6Zr alloy (~400 °C).

Finally, the severely deformed Ti−23Nb−0.7Ta−2Zr−1.2O alloy (a thickness reduction of 80%) manifests an excellent stability of the elastic modulus in the extremely large temperature range from −200 to 330 °C [24] (When the temperature increases beyond 330 °C, the alloy recrystallizes and reverts to a normal temperature dependence of its elastic modulus) Therefore, one can assert that the Ti−22Nb−6Zr in this study manifests a narrower range of the Elinvar behavior than the severely

deformed Ti−23Nb−0.7Ta−2Zr−1.2O alloy (~400 °C as compared to ~550 °C), but this behavior occurs at higher maximum temperatures (~550 °C as compared to ~330 °C), which represents an advantage for high temperature applications.

All discussed above make the observed two-way Elinvar behavior upon both heating and cooling in wide temperature range (ΔT=400 °C) in Ti−22Nb−6Zr alloy a quite unique phenomenon. The reason why some β-Ti alloys do not exhibit Elinvar effect, while the others can exhibit it in a single β-phase state, is not clear and requires additional study. However, such situation is not unique and is similar to the U−Mo alloys, where the Elinvar effect related to the single BCC β-phase is observed only in certain composition range [32].

5 Conclusions

(1) The Elinvar behavior observed in the Ti−22Nb−6Zr alloy is an example of the intrinsic (natural) Elinvar behavior of BCC β-phase due to its specific elastic atomic interactions. This fact was proven through physical torsional pendulum experiments, atomistic simulations and mechanical testing.

(2) The two-way intrinsic Elinvar behavior (both upon heating and cooling) can be obtained in Ti−22Nb−6Zr alloy in the 150−550 °C range under conditions when the heating/cooling rate is not lower than 9 °C/min, which suppress the ω-phase formation upon heating.

(3) Such Elinvar behavior with a temperature coefficient of f_r^2 being 10^{-5} °C^{-1} is stable, repeatable during thermal cycling in the Elinvar temperature range, and does not depend on the β-phase structure state, either polygonized dislocation substructure or recrystallized grain structure. The Elinvar behavior of the Ti−22Nb−6Zr alloy is not accompanied by the Invar behavior.

(4) The observed two-way Elinvar behavior opens up the way to practical use of the Ti−22Nb−6Zr alloy in high-temperature applications with sufficiently rapid temperature variations.

CRediT authorship contribution statement

Sergey DUBINSKIY: Conceptualization, Methodology, Investigation, Project administration, Writing − Review & editing; **Alexandra BARANOVA:** Investigation, Funding acquisition, Visualization, Data curation, Writing − Original draft; **Galina MARKOVA:** Investigation, Resources; **Anastasia ZELENINA:** Investigation, Visualization; **Lada KOLOTOVA:** Investigation, Visualization, Writing − Review & editing; **Sergey STARIKOV:** Investigation, Visualization; **Andrey KOROTITSKIY:** Methodology, Resources; **Andrey BAZLOV:** Methodology, Resources; **Sergey PROKOSHKIN:** Writing − Review & editing, Supervision; **Vladimir BRAILOVSKI:** Writing − Review & editing.

Declaration of competing interest

The authors declare that they have no known competing financial interests or personal relationships that could have appeared to influence the work reported in this paper.

Acknowledgments

A thermomechanical treatment and an X-ray diffraction analysis were carried out with the financial support of the Strategic Academic Leadership Program “Priority–2030” of NUST MISIS K6-2023-001. The calculations were carried out on the MVS-100K and MVS-10P computer clusters (RAS Joint Supercomputer Center).

Appendix A

The temperature dependences of the Young’s modulus of pure β-titanium calculated using the potential developed in this study were compared to the ab initio molecular dynamics (AIMD) calculations from Ref. [30]. It can be seen from Fig. A1 that both results are in a good agreement [30]. Consequently, the developed potential for titanium alloy is adequate and can be used for further simulations.

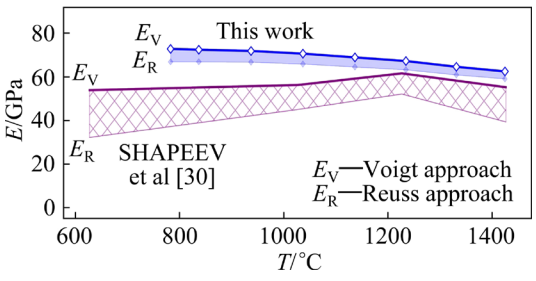

Fig. A1 Numerically simulated temperature dependences of Young’s modulus of pure β-titanium alloy: this work (MD calculations) and reference study (AIMD calculations) [30]

Appendix B

The Young's modulus (E) can be directly obtained from a torsional pendulum experiment using some mechanical calculations, mechanical testing results and RKM–TPI torsional pendulum specifications.

It is known that the Young's modulus (E) is related to the shear modulus (G) through the Poisson's ratio (v) by Eq. (B1):

$$E=G\cdot 2(1+v) \tag{B1}$$

For a square-shaped bar with a $b \times b$ cross-section and a rotation axis along length l, the shear modulus (G) is connected to the torsional moment (M) by Eq. (B2):

$$M=\frac{b^4 G}{6l} \tag{B2}$$

The torsional moment (M) can be obtained from the period of oscillation (t) through Eq. (B3):

$$t=2\pi\sqrt{\frac{I_{\text{total}}}{M}} \tag{B3}$$

where I_{total} is the moment of inertia of the whole system (moving parts of the RKM−TPI torsional pendulum and weights) and can be calculated as $I_{\text{total}}=I_{\text{w}}+I_{\text{inst}}$ (I_{w} is the moment of inertia of weights installed; I_{inst} is the internal moment of inertia of the moving parts of the RKM−TPI torsional pendulum).

The RKM−TPI torsional pendulum contains two ferromagnetic 0.06 kg weights mounted on a horizontal lever bar at a 0.06 m distance from the rotation centre corresponding to a moment of inertia $I_{\text{w}}=1.20\times10^{-3}$ kg·m^2. The internal moment of inertia of the moving parts of the RKM−TPI torsional pendulum is $I_{\text{inst}}=0.13\times10^{-3}$ kg·m^2. The final equation for the Young's modulus (E) is

$$E=\frac{48\pi^2(I_{\text{w}}+I_{\text{inst}})\cdot l\cdot(1+v)}{t^2\cdot b^4} \tag{B4}$$

where b is the width or thickness of the specimen, l is the working length of the specimen and v is the Poisson's ratio obtained in the experiment using a loading dilatometer (see the mechanical testing results).

References

[1] KIM H Y, HASHIMOTO S, KIM J I, HOSODA H, MIYAZAKI S. Mechanical properties and shape memory behavior of Ti−Nb alloys [J]. Materials Transactions, 2004, 45(7): 2443−2448.

[2] YONEYAMA E, MIYAZAKI S. Shape memory alloys for biomedical applications [M]. Cambridge: CRC Press, 2009: 352.

[3] BIESIEKIERSKI A, WANG J, GEPREEL M A, WEN C E. A new look at biomedical Ti-based shape memory alloys [J]. Acta Biomaterialia, 2012, 8: 1661−1669.

[4] KURAMOTO S, FURUNA T, HWANG J, NISHINO K, SAITO T. Elastic properties of gum metal [J]. Materials Science and Engineering A, 2006, 442(1/2): 454−457.

[5] AEBY-GAUTIER E, SETTEFRATI A, BRUNESEAUX F, APPOLAIRE B, DENAND B, DEHMAS M, GEANDIER G, BOULET P. Isothermal α'' formation in β metastable titanium alloys [J]. Journal of Alloys and Compounds, 2013, 577(Suppl.1): 439−443.

[6] BÖNISCH M, CALIN M, WAITZ T, PANIGRAHI A, ZEHETBAUER M, GEBERT A, SKROTZKI W, ECKERT J. Thermal stability and phase transformations of martensitic Ti−Nb alloys [J]. Science and Technology of Advanced Materials, 2013, 14(5): 055004.

[7] NIINOMI M. Mechanical biocompatibilities of titanium alloys for biomedical applications [J]. Journal of the Mechanical Behavior of Biomedical Materials, 2008, 1: 30−42.

[8] KIM H Y, FU J, TOBE H, KIM J I, MIYAZAKI S. Crystal structure, transformation strain, and superelastic property of Ti−Nb−Zr and Ti−Nb−Ta alloys [J]. Shape Memory and Superelasticity, 2015, 1(2): 107−116.

[9] SHEREMETYEV V, PETRZHIK M, ZHUKOVA Y, KAZAKBIEV A, ARKHIPOVA A, MOISENOVICH M, PROKOSHKIN S, BRAILOVSKI V. Structural, physical, chemical, and biological surface characterization of thermomechanically treated Ti−Nb-based alloys for bone implants [J]. Journal of Biomedical Materials Research, 2020, 108(3): 647−662.

[10] KIM J Il, KIM H Y, INAMURA T, HOSODA H, MIYAZAKI S. Shape memory characteristics of Ti−22Nb−(2−8)Zr (at.%) biomedical alloys [J]. Materials Science and Engineering A, 2005, 403(1/2): 334−339.

[11] MIYAZAKI S, KIM H Y, HOSODA H. Development and characterization of Ni-free Ti-base shape memory and superelastic alloys [J]. Materials Science and Engineering A, 2006, 438/439/440: 18−24.

[12] GASIK M M, YU H. Phase equilibria and thermal behavior of the biomedical Ti−Nb−Zr alloy [C]//Proceedings 17th Plansee Seminar. Reutte, Austria, 2009: 29.

[13] DUBINSKIY S M, MARKOVA G N, YUDINA E, PROKOSHKIN S D, BRAILOVSKI V. Elinvar effect in thermomechanically treated Ti−Nb−Zr alloy [C]//Proceedings of the European Symposium on Martensitic Transformations. Metz, France, 2019: 83−83.

[14] DUBINSKIY S, MARKOVA G, BARANOVA A, VVEDENSKIY V, MINKOVA I, PROKOSHKIN S D, BRAILOVSKI V. A non-typical Elinvar effect on cooling of a beta Ti−Nb−Zr alloy [J]. Materials Letters, 2022, 314: 131870.

[15] HARRIS B. The influence of some solutes on Young's modulus of niobium [J]. Journal of the Less Common Metals,

1967, 12(3): 247−250.

[16] Special Metals Corporation. NI-SPAN-C alloy 902 data sheet (Publication Number SMC-086). [EB/OL] [2004−09−04]. http:www.specialmetals.com/documents/technical-bulletins/ni-span-c-alloy-902.pdf.

[17] CAHN R W. An unusual nobel prize [J]. Notes and Records of the Royal Society, 2005, 59(2): 145−153.

[18] FEDOTOV S G, BELOUSOV P K. Elastic constants of titanium−niobium alloys [J]. Physics of Metals and Metallography, 1964, 17(5/6): 732−736.

[19] YANG Y, CASTANY P, CORNEN M, PRIMA F, LI S J, HAO Y L, GLORIANT T. Characterization of the martensitic transformation in the superelastic Ti−24Nb−4Zr−8Sn alloy by in situ synchrotron X-ray diffraction and dynamic mechanical analysis [J]. Acta Materialia, 2015, 88: 25−33.

[20] KIM H Y, WEI L S, KOBAYASHI S, TAHARA M, MIYAZAKI S. Nanodomain structure and its effect on abnormal thermal expansion behavior of a Ti−23Nb−2Zr−0.7Ta−1.2O alloy [J]. Acta Materialia, 2013, 61(13): 4874−4886.

[21] LAI M J, TASAN C C, ZHANG J, GRABOWSKI B, HUANG L F, RAABE D. Origin of shear induced β to ω transition in Ti−Nb-based alloys [J]. Acta Materialia, 2015, 92: 55−63.

[22] DENG Z, CHU K, Li Q, ONUKI Y, SUN Q. Elinvar property of cold-rolled NiTi alloy [J]. Scripta Materialia, 2020, 187: 197−201.

[23] ZHANG L X, WANG D, REN X B, WANG Y Z. A new mechanism for low and temperature-independent elastic modulus [J]. Scientific Reports, 2015, 5(1): 11477.

[24] SAITO T, FURUNA T, HWANG J H, KURAMOTO S, NISHINO K, SUZUKI N, CHEN R, YAMADA A, ITO K, SENO Y, NONAKA T, IKEHATA H, NAGASAKO N, IWAMOTO C, IKUHARA Y, SAKUMA T. Multifunctional alloys obtained via a dislocation-free plastic deformation mechanism [J]. Science, 2003, 300(5618): 464−467.

[25] QIN F Y, LU F S, CHEN Y L, YANG J M, ZHAO X Q. Deformation induced Elinvar behavior in Fe−Ni Invar alloy [J]. Science Bulletin, 2018, 63(16): 1040−1042.

[26] SONG Y W, JIN M, ZUO S, JIN X. Elinvar effect in severely-deformed Ti−50.8(at.%)Ni thin belt [J]. Materials Letters, 2019, 252: 96−99.

[27] QIU S, CLAUSEN B, PADULA S A, NOEBE R D, VAIDYANATHAN R. On elastic moduli and elastic anisotropy in polycrystalline martensitic NiTi [J]. Acta Materialia, 2011, 59: 5055−5066.

[28] AHADI A, KHALEDIALIDUSTI R, KAWASAKI T, HARJO S, BARNOUSH A, TSUCHIYA K. Neutron diffraction study of temperature-dependent elasticity of B19′ NiTi: Elinvar effect and elastic softening [J]. Acta Materialia, 2019, 173: 281−291.

[29] HE Q F, WANG J G, CHEN H A, DING Z Y, ZHOU Z Q, XIONG L H, LUAN J H, PELLETIER J M, QIAO J C, WANG Q, FAN L L, REN Y, ZENG Q S, LIU C T, PAO C W, SROLOVITZ D J, YANG Y. A highly distorted ultraelastic chemically complex Elinvar alloy [J]. Nature, 2022, 602(7896): 251−257.

[30] SHAPEEV A V, PODRYABINKIN E V, GUBAEV K, TASNÁDI F, ABRIKOSOV I A. Elinvar effect in β-Ti simulated by on-the-fly trained moment tensor potential [J]. New Journal of Physics, 2020, 22(11): 113005.

[31] SMIRNOVA D E, KUKSIN A Y, STARIKOV S V. Investigation of point defects diffusion in bcc uranium and U− Mo alloys [J]. Journal of Nuclear Materials, 2015, 458: 304−311.

[32] STARIKOV S, SMIRNOVA D. Details of structure transformations in pure uranium and U−Mo alloys: Insights from classical atomistic simulation [J]. Journal of Nuclear Materials, 2023, 576: 154265.

[33] CHANEY D, CASTELLANO A, BOSAK A, BOUCHET J, BOTTIN F, DORADO B, PAOLASINI L, RENNIE S, BELL C, SPRINGELL R, LANDER G H. Tuneable correlated disorder in alloys [J]. Physical Review Materials, 2021, 5(3): 035004.

[34] BARANOVA A, DUBINSKIY S, TABACHKOVA N, PROKOSHKIN S, BRAILOVSKI V. Kinetic features of the isothermal ω-phase formation in superelastic Ti−Nb−Zr alloys [J]. Materials Letters, 2022, 325: 132820.

[35] SHEREMETYEV V, BRAILOVSKI V, PROKOSHKIN S, INAEKYAN K, DUBINSKIY S. Functional fatigue behavior of superelastic beta Ti−22Nb−6Zr(at.%) alloy for load-bearing biomedical applications [J]. Materials Science and Engineering C, 2016, 58: 935−944.

[36] DUBINSKIY S M, PROKOSHKIN S D, BRAILOVSKI V, INAEKYAN K E, KOROTITSKIY A V, FILONOV M R, PETRZHIK M I. Structure formation during thermo-mechanical processing of Ti−Nb−(Zr,Ta) alloys and the manifestation of the shape-memory effect [J]. Physics of Metals and Metallography, 2011, 112(5): 503−516.

[37] DUBINSKIY S, PROKOSHKIN S, BRAILOVSKI V, INAEKYAN K, KOROTITSKIY A. In situ X-ray diffraction strain-controlled study of Ti−Nb−Zr and Ti−Nb−Ta shape memory alloys: Crystal lattice and transformation features [J]. Materials Characterization, 2014, 88: 127−142.

[38] NORMAN G E, STEGAILOV V V. Stochastic theory of the classical molecular dynamics method [J]. Mathematical Models and Computer Simulations, 2013, 5: 305−333.

[39] STARIKOV S V, KOLOTOVA L N, KUKSIN A Y, SMIRNOVA D E, TSEPLYAEV V I. Atomistic simulation of cubic and tetragonal phases of U−Mo alloy: Structure and thermodynamic properties [J]. Journal of Nuclear Materials, 2018, 499: 451−463.

[40] KLIAVINEK S S, KOLOTOVA L N. Modeling of glass transition process and elastic properties of Zr−Nb amorphous alloys [J]. Journal of Non-Crystalline Solids, 2021, 571: 121052.

[41] STARIKOV S, SMIRNOVA D. Optimized interatomic potential for atomistic simulation of Zr−Nb alloy [J]. Computational Materials Science, 2021, 197: 110581.

[42] ERCOLESSI F, ADAMS J B. Interatomic potentials from first-principles calculations: The force-matching method [J]. Europhysics Letters, 1994, 26(8): 583−588.

[43] SMIRNOVA D E, STARIKOV S V. An interatomic potential for simulation of Zr−Nb system [J]. Computational Materials Science, 2017, 129: 259−272.

[44] THOMPSON A P, AKTULGA H M, BERGER R, BOLINTINEANU D S, BROWN W M, CROZIER P S, IN'T VELD P J, KOHLMEYER A, MOORE S G, NGUYEN T D,

SHAN R, STEVENS M, TRANCHIDA J, TROTT C, PLIMPTON S J. LAMMPS: A flexible simulation tool for particle-based materials modeling at the atomic, meso, and continuum scales [J]. Computer Physics Communications, 2022, 271: 108171.

[45] VOIGT W. Textbook of crystal physics: Excluding crystal optics [M]. Berlin: B.G. Teubner, 1910: 964.

[46] REUSS A. Calculation of the yield point of mixed crystals based on the plasticity condition for single crystals [J]. Journal of Applied Mathematics and Mechanics, 1929, 9(1): 49−58.

[47] CROSSON R S, LIN J W. Voigt and Reuss prediction of anisotropic elasticity of dunite [J]. Journal of Geophysical Research, 1971, 76(2): 570−578.

[48] CHEN Q, SUNDMAN B. Calculation of Debye temperature for crystalline structures: A case study on Ti, Zr, and Hf [J]. Acta Materialia, 2001, 49(6): 947−961.

[49] MARKER C, SHANG S L, ZHAO J C, LIU Z K. Elastic knowledge base of bcc Ti alloys from first-principles calculations and CALPHAD-based modeling [J]. Computational Materials Science, 2017, 140: 121−139.

[50] MASUMOTO T, OHNUMA S, SUGAWARA K, KIMURA H. New type Fe−Mn based alloys with super Elinvar and Invar characteristics [J]. Materials Transactions, 2017, 58(4): 701−704.

[51] LU C, GONG D, JIA Y, ZHANG Y, SHEN Y, HOU W, MA N, LIU Z, YANG R, HAO Y. Achieving Elinvar effect over a wide temperature range in an additively manufactured titanium alloy [J]. Materials Research Letters, 2024, 12(12): 877−885.

[52] PROKOSHKIN S D, KOROTITSKIY A V, BRAILOVSKI V, INAEKYAN K E, DUBINSKIY S M. Crystal lattice of martensite and the reserve of recoverable strain of thermally and thermomechanically treated Ti−Ni shape-memory alloys [J]. The Physics of Metals and Metallography, 2011, 112: 170−187.

β型 Ti−22Nb−6Zr 合金在高、宽温域内的非典型本征 Elinvar 行为

Sergey DUBINSKIY [1], Alexandra BARANOVA [1], Galina MARKOVA [2], Anastasia ZELENINA [3,4], Lada KOLOTOVA [5], Sergey STARIKOV [6], Andrey KOROTITSKIY [7], Andrey BAZLOV [8], Sergey PROKOSHKIN [1], Vladimir BRAILOVSKI [9]

1. National University of Science and Technology “MISIS”, Laboratory of Shape Memory Alloys, 4 Leninskiy prospect, Moscow, Russia;
2. Tula State University, Department of Engineering and Materials Science, 92 Lenina prospect, Tula, Russia;
3. Moscow Institute of Physics and Technology, 9 Institutskiy per., Dolgoprudny, Russia;
4. Joint Institute for High Temperatures of RAS, 13 Bd. 2 Izhorskaya Street, Moscow, Russia;
5. National Research University Higher School of Economics, Faculty of Physics, 20 Myasnitskaya Street, Moscow, Russia;
6. Interdisciplinary Centre for Advanced Materials Simulation, Ruhr University Bochum, Germany;
7. National University of Science and Technology “MISIS”, Department of Physical Metallurgy of Non-Ferrous Metals, 4 Leninskiy prospect, Moscow, Russia;
8. National University of Science and Technology “MISIS”, Ultrafine-grained Metallic Materials Laboratory, 4 Leninskiy prospect, Moscow, Russia;
9. École de Technologie Supérieure, 1100 Notre-Dame Street West, Montreal, Canada

摘　要：对 Ti−22Nb−6Zr 形状记忆合金的 Elinvar 行为进行研究，旨在明确 Elinvar 行为的机制并找到控制该行为的方法。利用扭摆实验研究了弹性性能的温度依赖性，并利用 X 射线衍射分析方法评估了相组成的稳定性。通过压缩力学测试与经典原子模拟，分别在宏观和原子尺度上对所得结果进行了验证。结果表明，当加热/冷却速率≥9 ℃/min 时，该合金在 150~550 ℃范围内表现出双向 Elinvar 行为，其温度系数(f_r^2)约为 10^{-5} ℃$^{-1}$。无论合金具有多边化位错亚结构还是再结晶结构，该行为具有良好的稳定性与可重复性，且不依赖于 β 相的状态。研究得出结论：观察到的 Elinvar 行为是 BCC β 相的一种本征属性。

关键词：Elinvar 行为；β 钛合金；形状记忆合金；扭摆实验；原子模拟

(Edited by Wei-ping CHEN)